

SEMI-GLOBAL MATCHING: AN ALTERNATIVE TO LIDAR FOR DSM GENERATION?

S. Gehrke^a, K. Morin^b, M. Downey^a, N. Boehrer^c, T. Fuchs^c

^a North West Geomatics, Suite 212, 5438 - 11th Street NE, Calgary, Alberta, T2E 7E9, Canada -

{stephan.gehrke | michael.downey}@nwgeo.com

^b NovAtel Inc., 1120 - 68th Avenue NE, Calgary, Alberta, T2E 8S5, Canada - kristian.morin@novatel.com

^c Leica Geosystems AG, Heinrich-Wild-Strasse, Heerbrugg, CH-9435, Switzerland -

{nicolas.boehrer | thomas.fuchs}@leica-geosystems.com

Commission I, WG I/2

KEY WORDS: Surface, DEM/DTM, Aerial, Pushbroom, LiDAR, Algorithms, Matching, Orthorectification

ABSTRACT:

Airborne LiDAR has become the main technology to provide data for Digital Surface Models (DSM) and Digital Elevation Models (DEM) for various purposes, including orthorectification. At the same time, digital line scanners such as the ADS provide multiple stereo coverage, which can be used for image-based DSM/DEM derivation. Besides saving the LiDAR acquisition cost, such data provide several advantages over LiDAR results, especially since orthoimage generation can be based on the same data set. In that regard, North West Geomatics and Leica Geosystems have developed a DSM generation tool for ADS data. The underlying approach is Semi-Global Matching (SGM), which is suited for high-performance and high-resolution DSM computation. This paper presents the SGM approach for ADS and compares the results against LiDAR – in terms of data processing as well as DSM/DEM resolution and accuracy. The SGM and LiDAR properties are compared and exemplarily illustrated based on a sub-urban area in Romanshorn, Switzerland. It is shown that SGM can be used as an alternative to LiDAR. For certain applications such as high resolution DSM generation or orthoimage production in general – where it saves the additional flight costs – SGM is even considered the preferred choice.

1. MOTIVATION

In the last decade airborne LiDAR (Light Detection and Ranging) has established itself as a key technology to capture high resolution Digital Surface Models (DSM) and/or Digital Elevation Models (DEM). Over the same time the demand for higher accuracy and higher resolution DSMs/DEMs, delivered more frequently, has increased. LiDAR is a natural choice to fulfil this demand for various applications, including orthoimage production. However, the additional acquisition costs often prohibit its use solely for rectification. Considering the fact that imaging sensors like Leica Geosystems' ADS provide multiple stereo coverage, the image data itself can and should be used for photogrammetric DSM derivation. Therefore, in addition to LiDAR data acquisition and processing, North West Geomatics has developed a DSM generation tool from ADS line scanner imagery in cooperation with Leica Geosystems.

Generating a very high DSM/DEM resolution, in the order of the image ground sampling distance (GSD), presumes matching at the actual image resolution; or in other words: utilizing a per-pixel matching cost. Depending on image texture, a per-pixel measure is generally ambiguous; additional constraints, such as the assumption of a smooth surface, need to be introduced. Algorithms that globally minimize both cost and constraints are called global image matching; they are among the top-ranked matching approaches in terms of quality and resolution. Their drawback is performance, which is addressed by the Semi-Global Matching (SGM) approach of Hirschmüller (2005, 2008).

SGM approximates the two-dimensional, global aggregation of matching cost by a number of one-dimensional cost paths. It

still achieves similar accuracy as truly global matching but it is significantly faster – refer, e.g., to the systematic comparisons of SGM with local and global matching algorithms using different cost functions by Hirschmüller and Scharstein (2007, 2009). As a result, SGM has been further investigated and also enhanced by various researchers for different applications and data sets, including aerial images (Hirschmüller et al., 2005, Hirschmüller, 2008), terrestrial and extraterrestrial satellite data (Hirschmüller et al., 2006, Krauß et al., 2008, Alobeid et al., 2009) or video sequences (Heinrichs et al., 2007, Gerke 2008, Hermann et al., 2009). Furthermore, SGM is being recognized and deployed in the industry.

The SGM approach fulfils our need of high DSM resolution and high performance. Based on the quickly gaining mindshare and promising SGM results, we adapted the algorithm to the unique properties of ADS line scanner imagery using our existing software framework, in particular the highly optimized ADS sensor model.

The remainder of this paper describes the DSM derivation from ADS data based on SGM. The properties of SGM DSMs and derived DEMs are compared to LiDAR products, both in general and for an example data set that has been captured over the municipality of Romanshorn, Switzerland.

2. SEMI-GLOBAL MATCHING FOR ADS

SGM is a new image matching approach, which originates from the computer vision community. It has been developed by Hirschmüller (2005, 2008). The core algorithm aggregates per-pixel matching costs – for virtually all applications utilizing the

radiometrically robust Mutual Information – under consideration of smoothness constraints. The minimum aggregated cost leads to the disparity map (or, respectively, parallax map) for an image stereo pair, providing the corresponding location for each base image pixel on the respective epipolar line in the pair image. The SGM approach is suited for DSM collection in very high resolution, i.e. the image GSD.

2.1 Matching Cost: Mutual Information

SGM has been investigated with different cost functions, with the Mutual Information (MI) being favoured (Hirschmüller 2005, 2008, Hirschmüller et al. 2005, Hirschmüller et al. 2006). MI performed best for most cases in the comparisons by Hirschmüller and Scharstein (2007, 2009). Utilizing MI for image matching has been proposed by Viola and Wells (1997), mainly to handle complex images in terms of content but also illumination and viewing geometry, which is necessary for ADS data as well.

MI depends on entropy, which is a measure of the quantity of information needed to describe a signal. For individual images, radiometrically uniform areas have lower entropy than highly textured ones; joint entropy is a measure of similarity: Aligned images will have lower entropies than misaligned images – see Egnal (2000) for more detail. However, since two low-contrast areas will feature low entropy as well (even if misaligned), joint entropy itself is not sufficient as a cost function for matching. This leads to using MI, which combines individual entropies H_1 and H_2 and the joint entropy $H_{1,2}$ of base image I_1 and pair image I_2 , the latter of which warped by a disparity map D (Viola and Wells, 1997, Kim et al., 2003):

$$MI_{1,2} = H_1 + H_2(D) - H_{1,2}(D) \quad (1)$$

For single images, entropy is computed from the probability distribution of individual DN's, i.e. from a histogram. Similarly, the joint entropy is derived from a joint 2D histogram, which indicates how the DN's of image I_1 map to the DN's of image I_2 . (An ideal match with identical radiometry results in a straight, diagonal line of all histogram bins in the 2D space.) DN probabilities P – at base image pixel p and pair image location on the epipolar line provided by the disparity d – are derived from histogram counts and then converted into pixel-based entropy measures h according to Kim et al. (2003) and Hirschmüller (2005); for the joint entropy term:

$$h_{1,2}(p,d) = -\log[P_{1,2}(p,d) \otimes g] \otimes g \quad (2)$$

The Gaussian convolution g effectively performs Parzen estimation (Kim et al., 2003). According to equation 1, this leads to a pixel-based MI term (mi) and eventually to the matching cost c for any pixel combination given by (p,d) in a stereo pair (I_1, I_2), based on the fact that a good match between the images – which has to be assigned a low cost – results in high MI:

$$c(p,d) = -mi_{1,2}(p,d) = -h_1(p) - h_2(p,d) + h_{1,2}(p,d) \quad (3)$$

Thus, a cost matrix for all DN combinations can be computed and used as a look-up table for the SGM cost aggregation. Since an initial disparity map is required to warp the pair image towards the base image, the computation needs to be carried out iteratively (see below). We use a coarse seed DEM, $gTopo$, to provide an average disparity for MI initialization.

2.2 Cost Aggregation and Disparity Computation

The energy function $E(D)$ that has to be globally minimized consists of the actual matching costs c and smoothness constraints. Hirschmüller (2005, 2008) proposes to use the penalties P_1 for slight changes of one disparity and P_2 for any larger changes, i.e. discontinuities, in-between neighbouring pixels:

$$E(D) = \sum_p e(p,d) = \sum_p \left\{ \begin{array}{l} c(p,d) + \sum_{q \in N_p} P_1 T(|d - d_q| = 1) \\ + \sum_{q \in N_p} P_2 T(|d - d_q| > 1) \end{array} \right\} \quad (4)$$

The $T(\dots)$ function controls the application of penalties; it is 1 in case that its argument is true and 0 if false.

The theoretically desired two-dimensional cost minimization is approximated in SGM by multiple one-dimensional paths r , with $r = 8$, i.e. paths at every 45° , usually being sufficient (Hermann et al., 2009). These linear costs are aggregated over all pixels from each starting point p_0 to the opposite image border. The computation is carried out recursively, providing a linearly smoothed matching cost $l_r(p,d)$ at each base image pixel location p and each potential disparity d , following from equation 4:

$$l_r(p,d) = c(p,d) + \min \left\{ \begin{array}{l} l_r(p-r,d), \\ l_r(p-r,d \pm 1) + P_1, \\ \min_{i=d_{\min} \dots d_{\max}} l_r(p-r,i) + P_2 \end{array} \right\} \quad (5)$$

$$l_r(p_0,d) = c(p_0,d) \quad (6)$$

Within the minimum of the costs $l_r(p-r,\dots)$ at the previous pixel ($p-r$), the first term implies no disparity change compared to the current pixel p (without penalty), the second term allows for a small disparity change (with penalty P_1), and the last term regards all possible disparities (with penalty P_2) to model discontinuities. It has to be ensured that $P_1 > P_2$.

The overall cost $e(p,d)$ for each pixel p and disparity d results from the summation over all cost paths l_r :

$$e(p,d) = \sum_r l_r(p,d) \quad (7)$$

The disparity image D is obtained from the minimum summed cost for each base image pixel. Sub-pixel accuracy is achieved by fitting a quadratic polynomial, including the costs of neighbouring disparities, and computing the function's minimum. Because pixels at or close to the edges of the AOI are not fully constrained in all cost aggregation directions, for SGM computation we internally add 32 pixels at the borders, which are then clipped in the final result.

Following Hirschmüller (2005, 2008), disparity images are generated corresponding to the base image and also to the pair image by switching the role of base and pair image. This allows for a consistency check of the disparity map: Larger disparity differences ($d > 0.5$) indicate mismatches, which are predominantly caused by occlusions; respective results are voided. Out of the final processing steps as proposed by Hirschmüller (2008), we apply a 3x3 median filter to the disparity image and eliminate outliers based on segmentation, with the assumption that small segments of similar disparity (less than 50 pixels in size) most likely represent errors.

Note that the described cost aggregation does not require a seed DSM; it is designed to deliver results based on a given range of potential disparities. We decided to derive this range from the gTopo DEM, with applying a large buffer to account for inaccuracies and unmodeled objects such as buildings. SGM processing is carried out in image pyramids, mainly to allow a few iterations for MI initialization and disparity range reduction in the starting minification level of 8:1, where the processing is fastest. Afterwards, a single iteration per level is sufficient to refine the MI cost and derive SGM results in higher resolution.

2.3 ADS Line-Scanner Data: Considerations and Benefits

The ADS captures multiple panchromatic stereo image bands, which provide redundancy to fill gaps from occlusions as well as the ability for consistency checks between stereo pairs. Full colour (RGB) as well as NIR bands provide further stereo coverage along with additional radiometric properties, which can be beneficial for matching and also support post-processing (classification) of the results. The unique sensor geometry has to be regarded.

2.3.1 Epipolar Geometry: The projection of line scanners is central within each line and parallel in flight direction, with every scan-line featuring its individual exterior orientation. Even though a ‘perfect’, linear flight would result in straight, parallel epipolar lines, aircraft movements distort the imagery and accordingly the epipolar geometry. Most of these distortions are eliminated by pre-rectifying the original image data (L0) onto a plane (L1). While SGM is expected to generally benefit from using such L1 data, the major advantage over L0 is the possible approximation of the resulting epipolar curves as piecewise linear features. Similarly, these epipolar curves can be computed in a sparse pattern (4-16 pixels) with linear interpolation for pixels in-between, which makes both the epipolar grid initialization – based on the highly optimized ADS sensor model – and the time-critical epipolar point computation from disparity very fast.

2.3.2 Object Point Computation: A side-effect of the described epipolar grid setup is the intermediate step of 3D point computation for each line segment. Based on those points, final object points for all base image pixels can be derived by linear interpolation depending on disparity. This is significantly faster than performing forward intersections.

2.3.3 Multiple Stereo: Most configurations of the ADS provide three panchromatic stereo angles, in case of the ADS80: 14° backward, 2° forward and 27° forward. This results in three possible stereo pairs, although we do not use the largest viewing angle combination. That leaves two stereo pairs, with the nadir-most viewing angle providing the common base image. Then, either object points or disparity images can be joined, the latter of which requiring an intermediate object point computation. Although this seems extra work, the ‘detour’ of joining disparity images is preferred since it eases subsequent steps such as outlier elimination.

In this context it should be mentioned that the radiometrically flexible MI cost theoretically permits the use of the ADS colour bands, which would increase stereo coverage and potential matching quality (based on different radiometry). This possibility is subject to further research.

2.3.4 Handling of Large Image Takes: ADS L1 images are more than 12,000 pixels wide and can be up to 1,000,000 pixels long. This means that SGM processing needs to be carried out

on sub-tiles of, e.g., 1,024 x 1,024 pixels. Considering the ADS viewing angles and resulting stereo pairs, this size is just small enough to model a mountainous area or a downtown core in a fairly high GSD of 0.10 m – which might require in the order of 600-800 disparities – on a 64-bit system with 8 GByte memory; see Hirschmüller (2005) for details of SGM memory usage.

Based on the fact that results from a large number of takes have shown no evidence of tiling effects, the sub-tiles are processed independently without any overlap (apart from the area that is clipped already during processing – see above).

3. COMPARISON BETWEEN LIDAR AND SGM

LiDAR-acquired DSMs have become the standard for high-resolution surface generation. As an active sensor, LiDAR data can be captured regardless of light conditions (even at night) and the laser pulses can penetrate into forest canopy to measure the ground directly – a distinct advantage over competing techniques such as the image-based SGM. In addition to the elevation, LiDAR points often contain intensity information from the laser pulse, which can be plotted as an orthoimage. Due to a combination of sensing methods and geometry, LiDAR has a greater accuracy in height than in horizontal position; for high precision work typically 5 cm in Z and 10-15 cm in XY (Morin and El-Sheimy, 2001a). LiDAR point accuracy can also be affected by unmodeled atmospheric conditions (such as mist or volcanic ash) or by the reflectance properties of the target (Morin and El-Sheimy, 2001b).

As an emerging technology, SGM-derived DSMs are intended to be used as an alternative source of elevation and as a premier choice for ultra-dense surface extraction. DSMs are computed from imagery, which is typically acquired under strict mission constraints (sun angle, cloud cover, etc.); but as a derived product it does not add any cost to an imaging flight. Similar to LiDAR intensities, SGM points can be assigned the base image intensities and even the NRGB colour values based on the ADS source imagery. They can be plotted as an orthoimage. SGM accuracies are driven by the triangulation accuracies of the imagery – typically 0.5 GSD horizontally and 1.5 GSD vertically. In the case of ADS line scanner imagery, extreme turbulence can reduce the quality of the images and hence the derived SGM DSM. Table 1 gives a comparison between SGM and LiDAR in terms of data accuracy and properties as well as processing speed.

	LiDAR	SGM
Horizontal Accuracy	10-30 cm (altitude-dep.)	0.5 GSD
Vertical Accuracy	5 cm	1.5 GSD
Typical High Resolution	30 cm	5 cm
Surface Measured	top and ground	top
Processing Time	1,000,000 points/s	10,000-20,000 point/s

Table 1. Comparison between LiDAR and SGM.

For providing a DSM in a certain resolution, the acquisition time and cost for LiDAR is generally higher than for imagery, which forms the basis for SGM. Processing performance can vary widely for LiDAR and SGM, but in general SGM has a larger computation cost than LiDAR. This can be mitigated through the use of multi-threading, large scale cluster deployment and graphic processing units (GPUs) to accelerate the calculations. With the current CPU implementation, the SGM

processing achieves 10,000-20,000 points/s (Intel Core i7 @ 2.8 GHz), depending on disparity range. LiDAR processing speed is in the order of 1,000,000 points/s (2 x AMD Opteron 2220 @ 2.80 GHz; Leica Geosystems, 2009) – cf. Table 1. Both LiDAR and SGM methods result in high density digital surfaces, which typically require additional processing or editing before they can be used in an application. Data can be classified automatically to determine ground (DEM), buildings or vegetation content with minor changes to classification rules to accommodate the different point densities. The potentially higher density of the SGM DSMs can ease identification of structures in the data, making manual editing less error prone. On the other hand, LiDAR’s ability to penetrate canopy and supply multiple returns enhances its ability to determine the ground.

For the purpose of orthoimage generation, in addition to the obvious advantage of saving data acquisition costs there are distinct benefits of using image-based DSM generation: The geometry (datum) of the DSM is identical to the geometry of the images. Any adjustments made to the imagery – such as the triangulation – will be reflected in the DSM. Also, as the imagery and the DSM reflect the same time of recording, which means that the representation of the earth’s surface is consistent; any inaccuracies and noise due to temporal changes can be avoided. Lastly, as the SGM-generated DSM is created pixel-wise, the required resolution for orthoimage rectification is inherently provided.

4. EVALUATION RESULTS

SGM evaluation was undertaken using data from the Romanshorn municipality at Lake Constance in northern Switzerland. The imagery has been captured in the spring of 2007 using a Leica Geosystems ADS40, acquiring images at 5 cm GSD. The LiDAR DSM has been captured in the autumn of 2007 using a Leica Geosystems ALS50-II at a nominal point spacing of 30 cm. Imagery was adjusted with photogrammetric control and constrained with inertial navigation data (Sun et al., 2006). The estimated pixel accuracy is 2.5 cm in XY and 7.5 cm in Z. LiDAR data was adjusted to remove systematic errors (Morin and El-Sheimy, 2002) and co-registered with the imagery. The estimated LiDAR point accuracy is 15 cm in XY and 5 cm in Z. A subset of the area was chosen for SGM testing. It consists of a region with mixed urban areas, fields and water, 375 m x 475 m in size (Figure 1). There were ~1.5 million LiDAR points in this area. SGM resulted in ~63 million points based on ~74 million image pixels, which translates to 85% yield. To compare surfaces, the SGM and LiDAR DSMs were analysed in a commercial DSM package. Elevation differences were generated from unedited and ground-classified models and plotted to observe any systematic effects. Profiles were taken to highlight differences in urban areas (buildings, roads, etc.) and difference statistics calculated to judge performance.

The SGM-LiDAR comparison shows an average difference of $0.8 \text{ cm} \pm 5.4 \text{ cm}$. The small standard deviation suggests that the imagery and/or LiDAR data are more accurate than expected and that SGM potentially maximized its vertical accuracy. The difference plot in Figure 2 shows a number of areas (coloured white) larger than 3 GSD. In most cases these represent temporal effects such as grass pasture seasonal changes (large areas to lower left), construction (large rectangles) or changes in trees (random roundish shapes). Black areas contain no SGM data, mainly caused by occlusions; they naturally occur next to buildings and trees and, due to the sensor geometry, increase to-

wards the edges of the flight line, which are top and bottom in the difference plot.



Figure 1. Romanshorn test area overview from ADS RGB data.

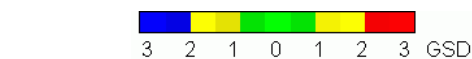
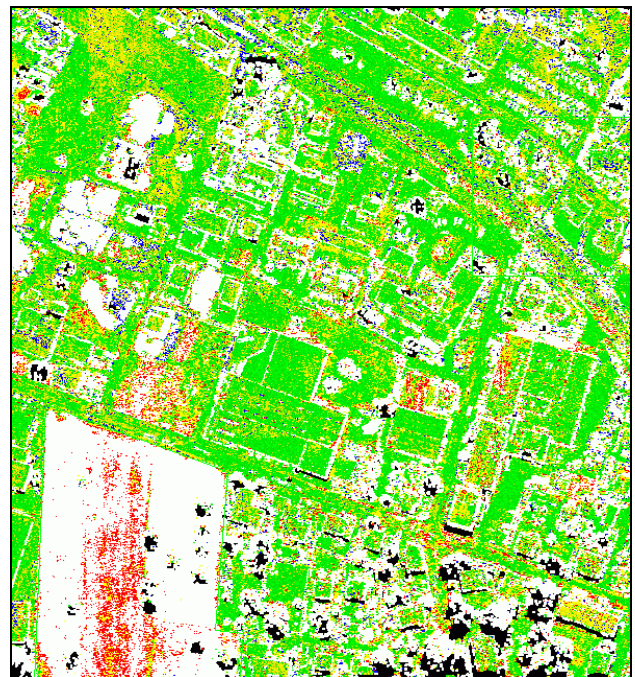


Figure 2. Difference plot between SGM and LiDAR DSMs.

The strong agreement between LiDAR and SGM results is supported by the profile (Figure 3), which shows a very good agreement between LiDAR and SGM points along man-made structures, and demonstrates some of the differences in trees while canopy heights are generally similar.

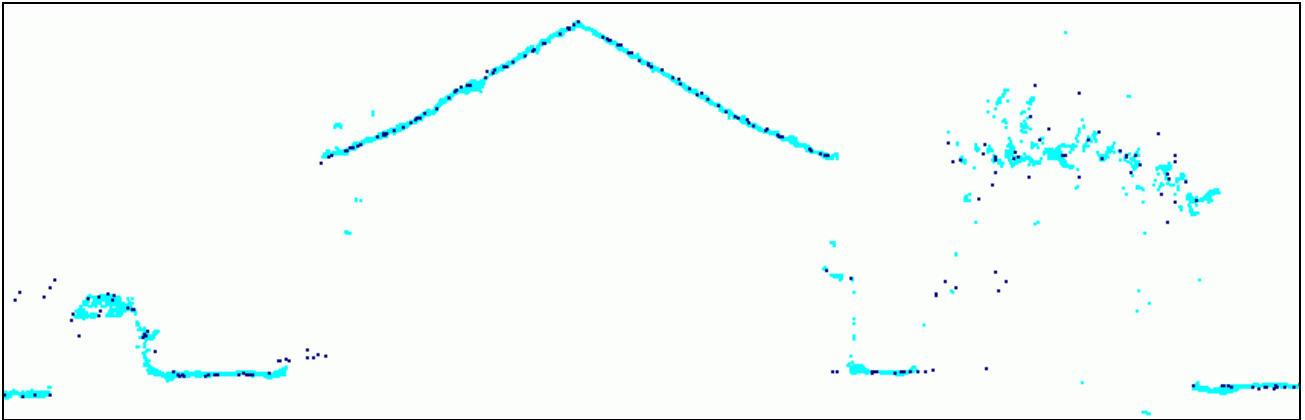


Figure 3. Profiles through SGM results (light blue) and LiDAR points (dark blue), containing a sidewalk, lawn, a house and trees.

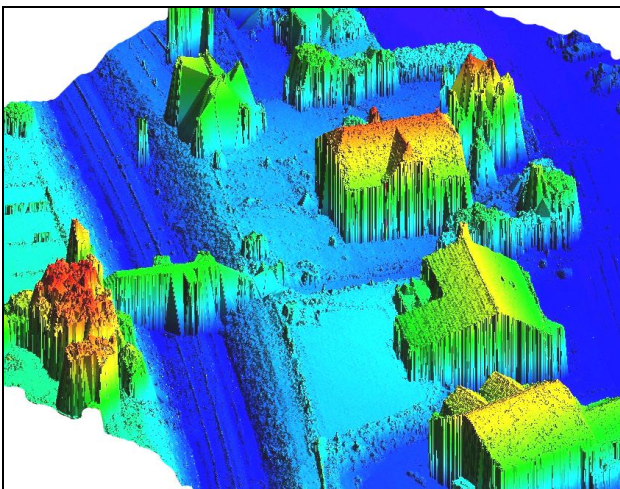


Figure 4. Detail of the SGM DSM in a perspective view.

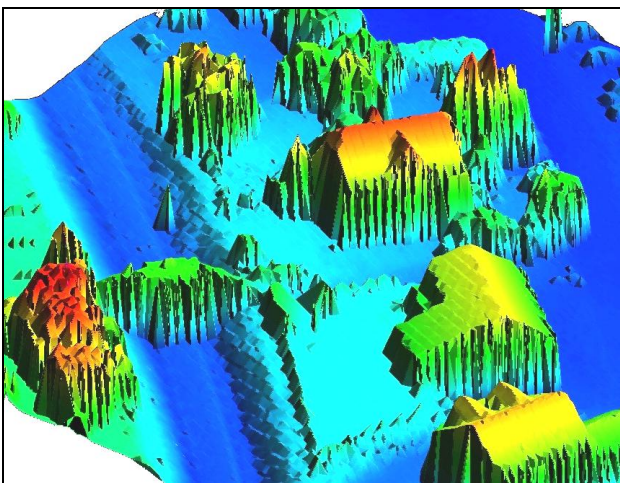


Figure 5. Detail of the LiDAR DSM in a perspective view.

A strength of pixel-based matching approaches like SGM is the behaviour at discontinuities, which is especially important in urban areas. In the comparison of perspective views – Figure 4: SGM, Figure 5: LiDAR – it can be seen that SGM has maintained sharp edges and also resolved a lot of detail on structures such as the railway tracks or the post next to them, which is not contained in the LiDAR data. (The object next to the railway in the LiDAR view – consisting of a single point – but not con-

tained in the SGM result is a bush. It indicates the LiDAR advantages at vegetation, whereas SGM might have not properly matched it and/or classified it as an error.)

Although not illustrated here, it should be mentioned that both LiDAR and SGM have non-desirable effects around water boundaries – LiDAR sometimes giving erroneous results due to penetration of the water surface and reflection of shallow bottoms. Based on smoothness constraints, SGM can bridge water areas through minimizing its disparity measure; however, this bridging can sometimes result in error.

5. CONCLUSION AND OUTLOOK

We presented a DSM derivation approach based on Semi-Global Matching (SGM) for ADS line scanner images and compared DSM and DEM results with LiDAR. It was found that the SGM-derived surface strongly agrees with the LiDAR points. Based on high resolution ADS imagery, the increased point density reveals fine detail that may be difficult for LiDAR to capture. There are, however, significant differences inherent to the respective method – generally around trees and vegetation, where LiDAR in contrast to image-based SGM has the ability to penetrate to the ground, or measure the top more consistently.

In conclusion, we have shown that SGM-derived DEMs/DSMs are revealed to be an effective alternative to LiDAR, especially when high resolution is a requirement. While both data sets can generally be used for the purpose of orthoimage rectification, SGM is the preferred choice as it is based on the same data set – representing the same point in time, identical geometry and resolution – and saves the additional acquisition cost of LiDAR. After extensive testing, SGM has just started to be used in North West Geomatics' production. Based on this practical experience and upcoming needs, the presented SGM approach will continue to be refined. The final goal is to seamlessly integrate the DSM generation into the ADS production work-flow.

6. REFERENCES

Alobeid, A., Jacobsen, K., Heipke, C., 2009. Building Height Estimation in Urban Areas from Very High Resolution Satellite Stereo Images. *ISPRS Workshop: High-Resolution Earth Imaging for Geospatial Information*, Hanover, Germany.

Egnal, G., 2000. Mutual Information as a Stereo Correspondence Measure. *Technical Report No. MS-CIS-00-20*. Univer-

sity of Pennsylvania, Department of Computer & Information Science.

Gerke, M., 2008. Dense Image Matching in Airborne Video Sequences. *The International Archives of the Photogrammetry, Remote Sensing and Spatial Information Sciences*, Beijing, China, Vol. XXXVII, Part B3b, pp. 639-644.

Heinrichs, M., Rohdehorst, V., Hellwich, O., 2007. Efficient Semi-Global Matching for Trinocular Stereo. *The International Archives of the Photogrammetry, Remote Sensing and Spatial Information Sciences*, Munich, Germany, Vol. XXXVI, Part 3/W49A, pp. 185-190 (PIA07).

Hermann, S., Klette, R., Destefanis, E., 2009. Inclusion of a Second-Order Prior into Semi-Global Matching. *3rd Pacific-Rim Symposium on Image and Video Technology*, Tokyo, Japan.

Hirschmüller, H., 2005. Accurate and Efficient Stereo Processing by Semi-Global Matching and Mutual Information. *Proc. IEEE Conference on CVPR*, New York, New York.

Hirschmüller, H., 2008. Stereo Processing by Semiglobal Matching and Mutual Information. *IEEE Transactions on Pattern Analysis and Machine Intelligence*, Vol. 30, No. 2.

Hirschmüller, H., Mayer, H., Neukum, G., and the HRSC Co-Investigator Team, 2006. Stereo Processing of HRSC Mars Express Images by Semi-Global Matching. *The International Archives of the Photogrammetry, Remote Sensing and Spatial Information Sciences*, Goa, India, Vol. XXXVI, Part 4.

Hirschmüller, H., Scharstein, D., 2007. Evaluation of Cost Functions for Stereo Matching. *Proc. IEEE Conference on CVPR*, Minneapolis, Minnesota.

Hirschmüller, H., Scholten, F., Hirzinger, G., 2005. Stereo Vision Based Reconstruction of Huge Urban Areas from an Airborne Pushbroom Camera (HRSC). *Proc. 27th DAGM Symposium*, Vienna, Austria, Vol. LNCS 3663, pp. 58-66.

Kim, J., Kolmogorov, V., Zahib, R., 2003. Visual Correspondence Using Energy Minimization and Mutual Information. *Proc. IEEE Conference on Computer Vision*, Vol. 2, pp. 1033-1040.

Krauß, T., Lehner, M., Reinartz, P., 2008. Generation of Coarse Models of Urban Areas from High Resolution Satellite Images. *The International Archives of the Photogrammetry, Remote Sensing and Spatial Information Sciences*, Beijing, China, Vol. XXXVII, Part B1, pp. 1091-1098.

Leica Geosystems, 2009. *Tech Note – Post Processing Times for ALS Data*.

Morin, K., El-Sheimy, N., 2001a. A comparison of airborne laser scanning data adjustment methods. *Proc. ISPRS WGII/2 Three-Dimensional Mapping from InSAR and LIDAR Workshop*, Banff, Alberta, Canada.

Morin, K., El-Sheimy, N., 2001b. The Effects of Residual Errors in Airborne Laser Scanning Terrain Data on Ortho-Rectified Imagery. *Proc. of Optical 3D Measurement Techniques V*, Vienna, Austria.

Morin, K., El-Sheimy, N., 2002. Post-mission Adjustment Methods of Airborne Laser Scanning Data. *Proc. FIG/ASPRS Annual Conference*, Washington, D.C.

Sun, H., Morin K., et al., 2006. IPAS – Leica Geosystems' High Accuracy GPS/IMU Integrated System for Airborne Digital Sensors. *Proc. ASPRS Annual Conference*, Reno, NV.

Viola, P., Wells, W.M. III, 1997. Alignment by Maximization of Mutual Information. *Int. Journal of Computer Vision*, Vol. 24, Part 2, pp. 137-154.